Title

Application of Synchrotron Radiation Techniques to Chemical Issues in the Environmental Sciences

Author

Allen, Patrick G.

Publication Date

1995-09-01

LBL-38370
UC-401

Lawrence Berkeley Laboratory
UNIVERSITY OF CALIFORNIA

CHEMICAL SCIENCES DIVISION

To be published as a chapter in *Application of Synchrotron Radiation in Industrial, Chemical, and Materials Science, American Chemical Society Monograph*, Washington, D.C., 1996

Application of Synchrotron Radiation Techniques to Chemical Issues in the Environmental Sciences

P.G. Allen, J.J. Bucher, M.A. Denecke, N.M. Edelstein, N. Kaltsoyannis, H. Nitsche, T. Reich, and D.K. Shuh

September 1995

Prepared for the U.S. Department of Energy under Contract Number DE-AC03-76SF00098

DISCLAIMER

LBL-38370
UC-401

Application of Synchrotron Radiation Techniques to Chemical Issues in the Environmental Sciences

Patrick G. Allen,[1,2] Jerome J. Bucher,[2] Melissa A. Denecke,[3]
Norman M. Edelstein,[2] Nik Kaltsoyannis,[2,*] Heino Nitsche,[3]
Tobias Reich,[3] and David K. Shuh[2]

[1]G.T. Seaborg Institute for Transactinium Science
Lawrence Livermore National Laboratory
Livermore, California 94551

[2]Chemical Sciences Division
Ernest Orlando Lawrence Berkeley National Laboratory
University of California
Berkeley, California 94720

[3]Forschungszentrum Rossendorf e. V.
Institute of Radiochemistry
P.O. Box 510119, D-01314
Dresden, Germany

*Present Address: Department of Chemistry
University College London
London, England WC1H OAJ

September 1995

This work was supported in part by the Director, Office of Energy Research, Office of Basic Energy Sciences, Chemical Sciences Division, of the U.S. Department of Energy under Contract No. DE-AC03-76SF00098. The work was performed in part at SSRL and NSLS which are operated by the U.S. Department of Energy, Office of Basic Energy Sciences, Divisions of Chemical Sciences and Materials Science.

APPLICATION OF SYNCHROTRON RADIATION TECHNIQUES TO CHEMICAL ISSUES IN THE ENVIRONMENTAL SCIENCES

Patrick G. Allen,[1,2] Jerome J. Bucher,[2] Melissa A. Denecke,[3] Norman M. Edelstein,[2] Nik Kaltsoyannis,[2,*] Heino Nitsche,[3] Tobias Reich,[3] and David K. Shuh[2]

[1]G.T. Seaborg Institute for Transactinium Science
Lawrence Livermore National Laboratory
Livermore, CA 94551

[2]Chemical Sciences Division
Lawrence Berkeley National Laboratory
Berkeley, CA 94720

[3]Forschungszentrum Rossendorf e. V.
Institute of Radiochemistry
P.O. Box 510119, D-01314
Dresden, Germany

*Present Address: Dept. of Chemistry
University College London
London, England WC1H OAJ

INTRODUCTION

The problem of hazardous waste contamination in the environment has become an issue of central importance in society. As the number of remediation efforts taking place worldwide grows and the public awareness of these problems increases, it is clear that the problems faced are enormous in terms of effort and cost. With existing chemical technologies being applied to well over one thousand contaminated sites within the U.S. alone, cost estimates for the cleanup efforts range well into the tens of billions of dollars. Furthermore, because many of the problems are still being assessed and identified, there is no accurate time estimate for the completion of these projects, with currently proposed restoration programs ranging well into the mid-21st century.

The types of contamination that have been recognized to date extend over the entire periodic table and include: Cd, Pb, Cr, Se, As, Zn, Cu, Ba, Ni, and Hg; radioactive Tc, Sr, and Cs as products of nuclear fission; radioactive Co resulting from activation; radionuclides U, Np, Pu, and Am; inorganic anions (NO_3^-, F^-, and CN^-); and a wide array of organics.[1-3] Depending on the physical form and chemical type of contamination, remediation strategies generally involve one or more of following technological disciplines: 1) characterization of the types of contaminants and their concentrations; 2) extraction, separation, conversion, or immobilization; and 3) containment

and storage (especially for radionuclides). Since many of the existing technologies, particularly those related to radionuclides, are still in their infancy, it is important to recognize that research and development can play a significant role in these long-term efforts. That is, with the tremendous expenditures of resources already planned, it is beneficial to conduct fundamental and applied research in each of the areas listed above to make the cleanup efforts more efficient, thereby reducing costs.

The purpose of this paper is to provide the potential synchrotron radiation (SR) environmental science user with an introductory level description of x-ray absorption spectroscopy and a brief overview of representative environmental investigations that have been reported to date. The narrative addresses the need, the utility, and fundamental principles of x-ray absorption spectroscopy techniques. The basic considerations for experimental work with samples of an environmental nature are also presented. This is followed by several short descriptions of the results from selected studies which are organized by the element of the environmental contaminant involved. The authors apologize in advance for the omission of the descriptions of a great body of superlative synchrotron radiation experimental work. This paper is not meant to be a comprehensive review, just an informative one. Many of these reviews emphasize the application of x-ray absorption spectroscopy techniques to materials containing radionuclides since this is the area of our expertise. There are also several examples taken from our research that were presented at the 1994 ACS Washington D.C. Meeting. Lastly, the future role of synchrotron radiation techniques in the environmental sciences is discussed before concluding.

CHARACTERIZATION

At each stage of remediation, a number of standard analytical techniques are commonly employed to determine the presence and concentrations of contaminants. Some examples of sensitive analytical methods are: inductively-coupled plasma atomic emission spectroscopy (ICP-AES), x-ray fluorescence (XRF), α, β, and γ spectroscopies (for radionuclides). However, in order to evaluate and improve upon existing remediation technologies, a more detailed knowledge of the speciation is required. Such information is generally obtained through the use of traditional spectroscopies such as; multi-nuclear nuclear magnetic resonance (NMR), UV-visible absorption/fluorescence, electron paramagnetic resonance (EPR), electron microscopies such as scanning electron microscopy (SEM) and transmission electron microscopy (TEM), photoacoustic spectroscopy (PAS), photoemission, and infrared and Raman vibrational spectroscopies. In the pre-treatment stage, determining the chemical form (i.e., phase, local environment, oxidation state) of the contaminant is important because the most effective remediation treatment is highly dependent on the exact form of the waste. During treatment, identifying the speciation is also required to determine the efficacy of the process being employed. Once a contaminant has been isolated for long-term storage, its speciation directly determines whether it can become mobile or reactive. In many instances, some of these methods may fail to differentiate between the same atom residing in different environments or oxidation states. In other cases, some techniques may be incapable of detecting a species in a particular form or oxidation state.

In addition to the traditional spectroscopic techniques mentioned above, methods based on the use of synchrotron radiation have proven quite valuable in addressing questions regarding speciation. In particular, x-ray absorption spectroscopy (XAS) techniques have been used extensively. XAS is an element specific structural technique which gives information on the average local structure around almost any atom. Since XAS originates from core level atomic-like transitions, a given atom will always exhibit characteristic x-ray absorption regardless of its speciation. In this regard, XAS may be viewed as a complementary tool to other molecular spectroscopies. The information derived from XAS studies is similar to crystallographic experiments (i.e., bond lengths and coordination numbers) with the important exception that XAS does not require long-range order (crystalline samples) and can be performed on amorphous solids or even on species in solution. This is a key point for the study of environmental samples where the element of interest often exists either as a surface adsorbed complex, in aqueous solution, or as

a colloidal suspension. The short description that follows is intended only to familiarize the introductory reader with the aspects of the basic technique.

Numerous detailed reviews of the XAS technique have been published elsewhere and the reader is referred to these for a more complete description of the experimental methods and procedures for data analysis.[4-6]

XAS BACKGROUND

Theory

The fundamental components of an x-ray absorption spectrum are centered around a sharp increase known as the absorption edge, which arises from a core-level electronic excitation. The detailed features that appear within ~20 eV above and below the main absorption edge are referred to as x-ray absorption near edge structure (XANES), and the features which lie ~20-1200 eV past the edge are referred to as extended x-ray absorption fine structure (EXAFS). The absorption edge is specific for a given element due to the unique core-level binding energies for each atom. The XANES region typically contains structure associated with transitions from core atomic states to bound molecular orbitals (valence or Rydberg) as well as to unbound states (continuum resonances). Because many of the transitions are between states where electronic selection rules may apply, XANES features can yield information about the electronic structure (density of states, oxidation state) and local geometry. At energies above the edge, absorption results in a transition to an unbound state of a photoelectron. The fine structure observed in the EXAFS region arises from a modulation in the absorption cross-section caused by interference between the outgoing and the backscattered photoelectron waves. The mathematical form describing the EXAFS which arises from N identical backscattering atoms at a distance R from the absorbing atom can be written as:

$$\chi(\mathrm{k}) = \frac{\mathrm{N}}{\mathrm{k}R^2}|f(\pi,\mathrm{k})|e^{-\sigma^2\mathrm{k}^2}\cdot\sin\left[2\mathrm{k}R+\phi_{as}+\pi\right]$$

where $|f(\pi,\mathrm{k})|$ is the backscattering amplitude, σ is the Debye-Waller damping factor, ϕ_{as} is the phase shift associated with the absorbing and backscattering atoms, and k is the photoelectron energy expressed as a momentum wave-vector in units of Å^{-1}. Curve-fitting is performed on raw $\chi(\mathrm{k})$ data or Fourier-filtered components of the raw data using $|f(\pi,\mathrm{k})|$ and ϕ_{as} functions that are derived either from model compounds of known structure or from theoretical calculations. Because the amplitude and phase functions are a function of atomic number, the types of near-neighbors may be determined to within Z ± 2-6. However, more often the identification of near-neighbor atom type can be made exactly with the help of other techniques or prior chemical knowledge. In general, curve-fitting analyses are able to determine the coordination numbers (N) and bond lengths (R) to within N ± 15 % and R ± 0.02 Å. In the case of two shells of the same backscatterer, Z, that are located at distances R_1 and R_2 from the central absorbing atom, the resolution is limited by $\Delta R \sim \pi/2k_{max}$. There has been great progress made in the theoretical modeling codes used to fit both EXAFS and XANES spectra. Perhaps the most widely known is FEFF6 developed by Rehr et. al.[7] Additionally, the computer codes used to reduce the raw absorption data continues to improve and an excellent example is the EXAFSPAK program suite developed by G. George.[8]

Data Acquisition

XAS spectra are typically measured either in transmission or as excitation spectra using fluorescence detection as shown schematically in Fig. 1. In transmission mode, a sample is placed between two gas-filled ionization chambers designated as I_0 and I_1. X-rays first pass through I_0,

then the sample and subsequently through I_1. The natural logarithm of (I_0/I_1) as a function of x-ray energy gives the characteristic absorption spectrum. Alternatively, the excitation spectrum is collected by measuring the x-ray fluorescence, which is proportional to the x-ray absorption coefficient. This is typically done by placing a detector, I_f, at a right angle to the axis of the incident beam. In this case, in principle, a plot of I_f/I_0 versus x-ray photon energy yields the same absorption spectrum as the one taken in transmission mode (the experimental geometry allows for simultaneous measurement). XAS spectra are energy calibrated by measuring the absorption spectrum of a well-known reference compound placed between I_1 and an additional ion chamber, I_2. For dilute samples (i.e., concentration < 1 wt.% or where the absorbance from the entire

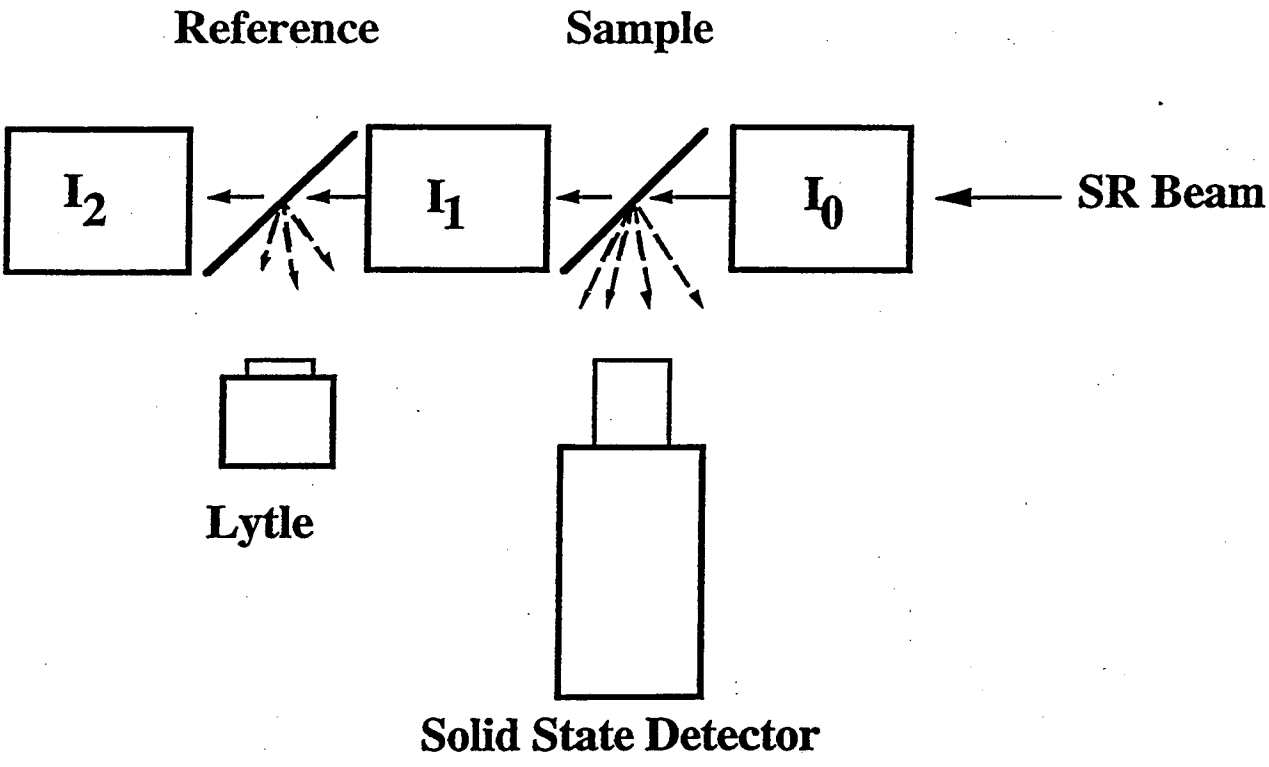

Figure 1. Schematic of an XAS experiment utilizing two fluorescence detectors.

sample is significantly greater than the absorbance from the element of interest) fluorescence detection is the detection method of choice due to its enhanced sensitivity over the transmission mode. In many environmental systems, fluorescence detection is the only suitable means of detection because of the extremely dilute concentrations of contaminants that are typically dealt with (~10-10^3 ppm).

The simplest means for detection of x-ray fluorescence from an element (atomic number Z) consists of a Soller-type slit and filter assembly in combination with an ionization chamber.[9] The combination Soller slit/filter unit (containing the element Z-1) preferentially absorbs scattered background radiation while transmitting the fluorescence line from element Z. This works well for systems that contain relatively few absorbers with well-separated fluorescence lines. However, in complex heterogeneous systems, there are frequently a multitude of elements at concentrations equal or greater to that of the contaminant which have fluorescence lines falling close to each other. In these cases, an energy dispersive detector may be better suited for resolving and isolating the desired fluorescence emission. Determination of the optimal detector system for a particular application depends on many factors and a complete analysis is presented in Ref. 10 by Warburton.

To date, the most commonly employed energy dispersive detector has been the thirteen element solid-state Ge array.[11] There are variations of these solid state arrays available depending on the energies and the counting rates being detected. However, features that are common to all include: pulse height processing, pulse shaping, and electronic discrimination. Single channel analyzers are used to define the appropriate energy windows for fluorescence signal collection. At low count rates, these detector systems can achieve resolutions of ~150 eV. At count rates approaching ~75 kHz, however, the resolution is degraded in favor of higher throughput. In general, these characteristics combined with signal averaging and the use of a high flux wiggler insertion device allow for collection of useful EXAFS data at concentrations as low as about 50 μM. Recently, Bucher et al.[12] have tested a novel design of a solid-state Ge detector and have demonstrated a practical detection limit approaching 5 μM. Development of new multi-element Ge and HgI systems possessing 25-100 detection channels, faster counting electronics, and third generation high brightness sources with increased flux should lower detection limits to further aid the study of environmental systems.

Sample Handling Requirements

The focus of this discussion is on environmental XAS techniques, thus many of the systems under investigation often contain toxic or hazardous species. Additional experimental safety requirements must be considered to ensure that experiments are conducted safely with minimal risk of exposure to anyone in the synchrotron radiation user facility or to the SR facility itself. Regardless of the exact nature of the environmental contaminant, the primary concerns involve proper documentation of all potential hazards, effective sample containment during the experiment, review of experimental procedures, and some level of monitoring for detecting accidental releases of the hazardous material.

Proper sample containment may be accomplished through the use of a multi-layer container system which is kept sealed at all times. The operative design principle is the presence of redundant, engineered multiple barriers so that in the event that one layer of protection should fail the sample isolation and integrity will be maintained. The challenge is to design and engineer a sample cell out of materials that will simultaneously allow x-rays to enter and exit without appreciable attenuation, while at the same time maintaining an adequate hermetic seal. Many common designs used to date have borrowed from cryogenic and vacuum techniques where the problems associated with materials compatibility (mating plastic or glass windows to metal frames) have already been solved.

The issue of sample containment and monitoring is particularly relevant to working with radionuclides. Monitoring is necessary before, during, and after an experiment. The degree of monitoring effort depends on the nature of the sample and the experimental conditions under which the study is performed. Thus, specialized experiments utilizing temperature as a variable or experiments involving *in-situ* chemical modification of the sample can become more time consuming from a safety engineering perspective. Monitoring of radionuclides is complicated further when considering the different isotopes and their modes of decay. For example, ^{239}Pu is primarily an alpha emitter which makes it less of a radioactive hazard if exposure is only external since the alpha particles are stopped by the outer dead layer of skin. However, ^{239}Pu absorbed internally is highly toxic as the alpha particles are now in contact with living tissue and can cause cancer. In contrast, ^{137}Cs is a strong gamma emitter and thus poses a significant external hazard resulting from the large radiation field. The type of monitoring (α, β, or γ) needs to be tailored to the specific radionuclide. Therefore, the overall safety measures required for each experiment must be reviewed and examined on a case-by-case basis for each experimental system.

ENVIRONMENTAL APPLICATIONS OF XAS

Selenium

Hayes and coworkers have reported a study of selenium adsorption on α-FeOOH (goethite) using XAS at the Se K-edge.[13] In studying the adsorption of selenite and selenate at the α-FeOOH-water interface, they found that selenate adsorbs as a weakly bonded outer-sphere complex while in contrast, selenite adsorbs as a strongly bonded inner-sphere complex. Pickering and coworkers investigated selenium on contaminated soils from the Kesterson Reservoir in California.[14] These results demonstrated that elemental selenium is present in the contaminated soils and in simulated soil experiments. These findings are important in determining transport properties because the mobility (solubility and binding constants) is largely dependent on the chemical form (i.e., reduced selenium is less mobile than the oxidized forms).

Cobalt

O'Day, Chisholm-Brause, and coworkers have reported several XAS investigations of Co chemisorption on oxide surfaces.[15-19] The primary goal of this work was to characterize the dominant form of surface complex under specific coverage conditions and to gain some insight into the mechanisms of partitioning at the solid/water interface. They studied Co(II) sorbed on γ-Al_2O_3, rutile (TiO_2), α-SiO_2, and kaolinite ($Al_2Si_2O_5(OH)_4$). The results established the presence of multi-nuclear as well as mononuclear sorption complexes, whose relative amounts depended on surface coverage. Furthermore, the bond lengths and coordination numbers of the surface complexes were found to be different depending on the type of surface. For example, on kaolinite at low coverages, Co(II) binds strongly as an mononuclear inner-sphere complex. At higher coverages (still below one monolayer of Co), oxy- or hydroxy-bridged polynuclear species are formed.

Hayes and coworkers have also investigated Co(II) adsorption on oxide surfaces with an emphasis on the effect of mixed cation/anion systems (i.e., Co/Se).[20] The utility of acquiring accurate structural data on surface complexes lies in being able to predict transport behavior using macroscopic surface complexation models (SCM). In these examples, the transport properties are dramatically different for mononuclear versus multi-nuclear complexes, and as a result the information on the nuclearity of the surface species is critical to developing accurate models. This type of approach is essential for evaluating and devising innovative waste remediation techniques.

Chromium

Bidoglio and others have recently studied the mechanism of Cr adsorption on iron oxide minerals (goethite).[21] Using XANES measurements at Cr K-edge, they determined that adsorbed Cr(VI) ions are partially reduced to Cr(III) on the α-FeOOH surface under oxygenated conditions. The structure of Cr(III) ion sorbed on goethite has been described by Charlet and Manceau.[22] In this work, it is shown that a γ-CrOOH precipitate is formed at the surface under conditions well below saturation. A similar result was found by Fendorf et al.[23] for Cr(III) adsorbed on silica in that a γ-CrOOH surface precipitate was formed below monolayer coverage and at conditions where solution precipitation does not occur.

Lead

Chisholm-Brause, Hayes et al. have investigated the structure of Pb(II) surface complexes at the γ-Al_2O_3 and α-FeOOH (goethite)-water interfaces.[24-25] The Pb L_{III}-edge XAS results on α-FeOOH indicated that the sorption mechanism is strongly influenced by the concentrations of the sorbate. At low coverages, monomeric surface complexes are formed, while the formation of extended polymeric species is indicated at higher coverages. Similarly, Pb(II) bonds directly to γ-Al_2O_3 as a mononuclear, inner-sphere complex, with the formation of small polynuclear species

occurring only as the coverage is increased. In either case, the data did not reveal any evidence that indicated the formation of a solid precipitate. These results demonstrate the utility of XAS for differentiating between mechanisms of adsorption, (i.e., inner-sphere versus outer-sphere complex formation).

Inorganic Elements From Fossil Fuels and Sediments

The presence of toxic inorganic elements in fossil fuels is a problem since the combustion process provides a mechanism for the release of these elements into the environment, either directly into the air, or by the leaching of combustion waste into the groundwater. Knowledge of speciation is crucial since the toxicity of many of these elements depends on their oxidation state. Silk and coworkers[26] have used XAS to investigate the chemical form of arsenic, nickel, and vanadium in oil fly-ash samples. Their results showed that the principal oxidation states that are present for each element are V(IV), Ni(II), and As(V).

Huggins and coworkers[27] have studied the speciation of chromium and arsenic in coal and coal ash. The results show that the chromium exists in the trivalent oxidation state in all samples. The Cr K-edge XANES of the coal samples demonstrate the presence of an oxyhydroxide, i.e., CrOOH, while the speciation in the ash is dominated by a form indicative of chromium in a silicate mineral. Arsenic K-edge XAFS show that As exists substitutionally for the element sulfur in pyrite (FeS_2). Arsenate (AsO_4^{3-}), possibly derived from the oxidation of arsenic contaminated pyrite, is also found in some coals as well as ash.

Vairavamurthy et al.[28] have studied the effects of hydrogen sulfide and thiols on the speciation of chromium, nickel, and copper in anoxic marine sediments. Since such sediments may serve as a sink for toxic metals, marine sediments can act as a source and carrier for the redistribution of toxic species. XAS studies at the Cr, Ni, and Cu K-edges showed that various redox processes were occurring. For example, Cr(VI) is transformed to Cr(III) by a commonly occurring thiol, while Ni(II) and Cu(II) remain inert to the same treatment. Hydrogen sulfide apparently does not reduce Cr(VI), Ni(II), or Cu(II), but instead causes some structural rearrangements to occur primarily in Ni(II) and Cu(II).

RADIONUCLIDES

Strontium

Radioactive ^{90}Sr produced from nuclear fission poses another health hazard in the environment. Pingitore and co-investigators have studied the mode of incorporation of Sr^{2+} into calcite using XAS.[29] They have found that Sr^{2+} enters the calcite lattice substitutionally adopting a structural environment with six-fold coordination similar to that of the Ca^{2+} lattice sites. The results suggest that incorporation of Sr^{2+} occurs through formation of a dilute solid solution rather than through adsorption or occlusion. In addition, since it is substitutional for Ca, it is not likely to be significantly more mobile than Ca. Preferential leaching of Sr from calcite is not anticipated and any encapsulated Sr should be relatively immobile which has important implications for ^{90}Sr in similar environments. Kohn et al.[30] have reported a similar study relevant to Sr partitioning in dry and hydrous silicate glasses. They find that the Sr-O bond distances are shorter than for crystalline silicates and appear to shorten with decreasing polymerization. Hydration of the dry glasses seems to increase the Sr-O bond lengths. These minor changes in the first shell coordination suggest that the Sr partition coefficients are not strongly dependent on melt composition.

Uranium In Contaminated Soils

XAS has recently been used by Conradson et al.[31] to study the adsorption of uranium on contaminated soils at the Feed Materials Production Center in Fernald, Ohio. This site served as a uranium processing plant operating as part of the DOE weapons program. Over a 30 year period,

varying amounts of uranium were distributed around the site leaving concentrations in excess of 1000 ppm at some areas. Along with laser-induced luminescence spectroscopy, XAS measurements at the U L_{III}-edge showed that ~80-90 % of the uranium from all of the areas on the site was present in the uranyl form (uranium in a (VI) oxidation state containing the linear UO_2^{2+} moiety). Based on these and other results, numerous treatments were considered and tested for their efficiency of uranium removal. Most of the methods that were tested utilized a chelating agent such as carbonate, citrate, or Tiron as a method for extracting the uranyl species. Variations of these processes involved the addition of a reducing agent like sodium dithionite to promote dissolution. Based on characterizations of the uranium that remained on the soil subsequent to the various treatments, several different effects were observed in the soils. Treatment with water or dithionite had essentially no effect on removal and served as a control. All other treatments served to decrease the total amount of uranium in addition to increasing the relative amount of U(IV)-containing species (such as UO_2) that remained on the soil.

Bertsch et al.[32] have also used XAS to determine the speciation of uranium in contaminated soils and sediments from the Fernald Environmental Management Project and the Savannah River Site. In this work, the x-ray beam was adjusted from 50-300 μm spot sizes, which enabled the experimenters to spatially resolve differences in the distribution of uranium oxidation states. Based on the edge position and spectral signatures associated with the U L_{III}-edge, they found that the uranium in all of the clay fractions was predominantly in the U(VI) form. The lack of spatial variation was attributed to the individual clay particles being much smaller than the beam size. In contrast, spatial variability was seen on the sand samples taken from both sites. They observed two general types of domains: 1) regions that contained primarily U with unusually small amounts of other elements such as Fe and Mn; and 2) regions that were depleted in uranium yet relatively enriched with Fe and Mn. In addition, they also observed variations in the oxidation state among the sand and silt fractions taken from the Fernald site. These amounted to regions of predominantly U(VI) or U(IV), as well as mixtures of these two oxidation states. The presence of U(IV) in the Fernald sand and silt samples was attributed to U(IV) being in the source term as an airborne particulate rather than as soil-reduced U(VI).

Uranium Sorption

Another example of the application of XAS to determine speciation is given in a series of investigations of uranium adsorbed on the mineral montmorillonite. Chisholm-Brause et al.[33] studied the sorbed complex structure as a function of uranium surface coverage. They found that over a 20-fold range of surface coverages, there were systematic changes in the coordination numbers and bond lengths for the oxygen atoms in the equatorial planes of the sorbed uranyl species. This behavior was attributed to the existence of at least three structurally distinct sites on the clay that were interacting with uranyl over the range of coverages studied. Dent et al.[34] also found that the uranyl ion retains its structure after adsorption onto montmorillonite. However, in their study they observed changes in the surface complex structure as a function of varying pH. At pH <3 a monomeric aquo-complex consisting of the uranyl ion with 5-6 equatorial oxygens is observed, while at pH of 4.3 the data indicate the presence of a multi-nuclear species. These results taken together have significant implications for developing accurate transport models and illustrate the valuable microscopic information that is readily available from XAS.

Uranium Bioremediation

Dodge and coworkers[35] recently investigated uranium reduction by *Clostridium* sp. using XANES and x-ray photoelectron spectroscopy (XPS). Comparisons of XPS spectra for U(VI) in the control sample and the U in the sample inoculated with *Clostridium* sp. showed that U(VI) was reduced to U(IV). Analysis of the uranium XANES at the M_V-edge for U metal, UO_2, and the inoculated sample also confirmed the reduction of uranium. Their results further showed that the reduction only occurred in the presence of live or growing cells, suggesting the reduction occurs through enzymatic action.

Actinides In Silicate Glasses

Farges et al. have studied the local structure of trace to minor levels of uranium in various silicate glass/melt systems using XAS.[36] Depending on the glass compositions and the oxidizing or reducing conditions, the syntheses generally yielded uranium with oxidation states of (IV), (V), or (VI). They found that the U(VI) sites were composed of uranyl groups with two axial oxygen atoms at 1.77-1.85 Å and four to five equatorial oxygens at 2.21-2.25 Å. The U(V) was found to occur in distorted polyhedra with six oxygen atoms at 2.19-2.24 Å. The U(IV) sites, although similar to the U(V) sites, have less distortion about the octahedra and have six oxygens at 2.26-2.29 Å. In the syntheses which included minor amounts of F or Cl, no evidence for uranium-halogen coordination was found. In most cases, there was no indication of uranium second nearest neighbors that would suggest any amount of local clustering. In addition, more detailed XAS analyses of the bond lengths and strengths afforded some plausible explanations of the compatibility and solubility of uranium in the melt.

Eller, Larson, and coworkers[37-38] performed XAS investigations of the coordination environment of uranium, thorium and selected lanthanides (Ce, Pr, Gd, and Lu) in borosilicate glass, a medium which has been chosen for the storage of high-level radionuclide waste. The study of lanthanides is relevant because they serve as structural models for the trivalent actinides. Based on the U L_{III}-edge XANES position as well as optical measurements, uranium was found to be present in the glass in the hexavalent form, although there was no evidence for the uranyl structure (2 short axial oxygens) as is found for most U(VI) oxide species. Such a finding is not without precedent in that cubic UO_3 also exists in a non-uranyl, non-localized form. Under conditions of higher uranium loadings in silicate glasses, other groups[39-41] have found that U(VI) formed uranyl-type multi-nuclear clusters. Np(V) apparently behaves similarly to U(VI) and also forms actinyl structures in these glasses. The structure of the tetravalent ions of U, Np, and Pu resemble the fluorite structure of UO_2 with coordination numbers ranging from 6-8. In the case of the lanthanides, each was found to enter the glass primarily in the trivalent oxidation state (Ce may exist as 4+), with well-ordered first shells of oxygen neighbors.

Barret et al.[42] used fluorescence XAS at grazing incidence to investigate changes at the surface of borosilicate glasses containing 3 wt.% uranium. Comparison of the spectra taken at grazing incidence with those of the bulk glass allows detection of structural differences at the surface. Performing the XAS measurements *in-situ* during aqueous leaching at 100°C, they found a local increase in uranium concentration at the surface during the first 30 minutes. The surface structure was composed of polynuclear clusters composed of uranyl-like sub-units. The clusters were partially removed after 30 minutes.

Neptunium Sorption On Goethite

Brown and co-investigators reported a study of Np(V) adsorption at the α-FeOOH (goethite)/water interface.[43] Based on a comparison with Np and U L_{III}-edge XAS data taken for several model systems, the Np(V)-goethite sample was determined to sorb as the neptunyl moiety (NpO_2^+). Curve-fits to the EXAFS data gave two oxygens at 1.85 Å and ~5 equatorial oxygens at 2.51 Å indicative of a distorted pentagonal-bypyramid. While the data indicated no formation of multi-nuclear species, a second shell feature in the data was tentatively assigned to a Np-Fe interaction which would suggest an inner-sphere coordination complex.

Actinide Near-edge Structure

Several groups have performed detailed investigations of U, Np, and Pu XANES (L_{III}; $M_{III,IV,V}$; $N_{IV,V}$; and $O_{IV,V}$ edges) for a variety of solid compounds with different oxidation states.[44-47] One of the key issues under consideration is the assignment of oxidation state based on the L_{III} absorption edge position. In nonmetallic systems (particularly oxides and halides), differentiating between the oxidation states (III), (IV), and (VI) for Np and U is fairly well-

established by chemical shifts plus spectral signatures. Another issue studied in some detail is the characteristic shoulder present on the high-energy side of L_{III}-edges of uranyl- or neptunyl-containing compounds. Because it is consistently observed in the L_{III}-edges of these compounds, this spectral feature has been used as a signature for the uranyl or neptunyl groups. It has also been postulated that this feature arises from a multiple-scattering resonance associated the linear UO_2^{2+} or NpO_2^{+} groups.[44] Since the uranyl- or neptunyl-containing systems also possess the U(VI) or Np(V, VI, VII) oxidation states, the shoulder has also been used as a indicator for oxidation state. Along these lines, it has been argued that the shoulder results from an electronic effect related to multiple *5f* final state configurations rather than a multiple scattering resonance.[47]

Plutonium In Concentrated Nitric Acid

Information on the speciation of Pu(IV) in nitric acid is required in order to improve the efficiency of current aqueous separations techniques (extractions and ion-exchange) of the actinides. Veirs et al.[48] have recently reported the structural determination of the aqueous nitrate complexes of Pu(IV). Solutions of the Pu(IV) ion were studied in nitric acid concentrations of 3, 8, and 13 M. Systematic changes in the EXAFS demonstrated the trends of increasing nitrate ligation and decreasing water ligation as a function of increasing nitric acid concentration. The coordination numbers of the nitrogens and non-coordinating oxygens were found to be consistent with previous UV-visible absorption studies in which the principal species were found to be the di-, tetra-, and hexanitrato complexes in these solutions. The Pu(IV) complexes in nitric acid have structures which are similar to analogous solid state compounds of thorium and neptunium nitrate compounds. The results indicated that the nitrate ligands are planar and bidentate. Furthermore, the nitrate structure was found to be distorted with respect to that of the free nitrate in that the nitrogen-oxygen bond length of the non-coordinating oxygen is significantly shorter than the nitrogen-oxygen bond lengths of the coordinated oxygens.

Plutonium Metallurgy

Another important area of plutonium research involves aspects of the stability of its metallic phases. Plutonium has a complex phase diagram possessing six phase transformations and several different crystal structures between room temperature and its melting point. Phase stabilization at low-temperature is an important requirement for fabrication and long-term storage. At ambient temperature, the fcc δ-phase is stabilized by adding low concentrations of gallium or aluminum. The mechanism of this stabilization is still unknown. Cox et al.[49] have investigated the local structure of the gallium and plutonium environments in 1 wt.% Ga δ-stabilized plutonium. XAFS measurements were performed at the Ga K-edge and Pu L_{III}-edges at 80 K. The results of this study showed that the Ga substitutes isomorphically in the fcc lattice. The structure around the Ga atoms is well-ordered with a first shell of 12 Pu neighbors at 3.14 Å. In contrast, the Pu environment is extremely disordered with an average first shell distance of 3.29 Å, which is close to the value expected for the pure δ-phase metal. A model for the fcc lattice stabilization is proposed in terms of the local $GaPu_{12}$ clustering.

RESEARCH FROM THE LBNL ACTINIDE CHEMISTRY GROUP

Selenium Bioremediation

The concentration and immobilization of hazardous materials by microbial agents offers great potential for use in environmental remediation technologies.[50,51] In the case of selenium possible future applications of bioremediation technologies range from oil refinery waste streams containing selenite to agricultural drainage which has contaminated sites such as the Kesterson Reservoir in California. The aerobic soil bacterium, *Bacillus subtilis,* has been found to detoxify selenite, Se(IV), by reductive metabolization although the exact mechanism is not fully understood.[52] As in

other cases selenium oxyanions appear to be reduced to a red elemental form, although there is no direct *in situ* spectroscopic evidence to support this contention.[53,54]

Vegetative cells of *B. subtilis* and of an unidentified bacillus isolated from the Kesterson Reservoir were exposed to aqueous growth media containing either selenite or selenate. The bacteria metabolized the selenite growth solution, however, there was no uptake of selenium in the selenate solution. In addition to the isolated bacterium, selenium K-edge XANES spectra were obtained for elemental selenium (red and gray allotropes), Na_2SeO_3,and Na_2SeO_4 powders, all of which contain selenium in well-defined oxidation states. The edge positions in selenite and selenate are shifted to higher energy by 4.2 and 9.0 eV respectively, relative to elemental selenium (at 12658 eV). Figures 2-3 (Se K-edges and chemical shifts, respectively) show the XANES of red and gray selenium together with those of the bacteria, and clearly demonstrate that the selenium is present in elemental form in both *B. subtilis* and the Kesterson bacillus. There is also a discernible difference between the red and gray allotropes of selenium in the near edge region (12665-12675 eV). The results suggest that both *B. subtilis* and the Kesterson bacillus reduce selenite to red selenium, a finding consistent with the assertion that red selenium is the biological end product. These results support the view that organisms like *B. subtilis* offer a promising means for the removal of selenite from contaminated aqueous environments such as oil refinery and agricultural waste streams.

The origin of the XANES difference between gray and red selenium is not easy to ascertain. Although the theoretical modeling of XANES has become widespread, it is very difficult to achieve without well-established structural parameters. Unfortunately these are not available for selenium. Elemental selenium occurs in a number of structural modifications, not all fully characterized, and often in a mixture of phases. The gray "metallic" form is thermodynamically the most stable and consists of unbranched helical chains with Se-Se distances of 2.37 Å. Red selenium has three

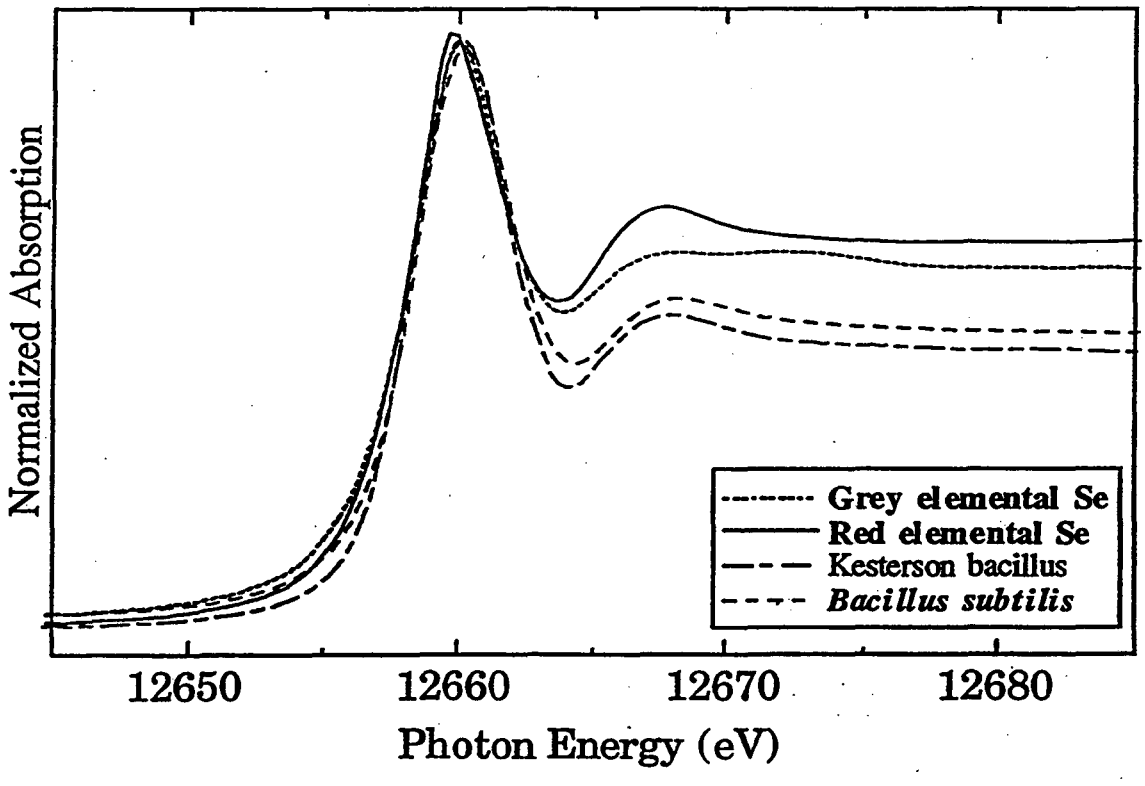

Figure 2. Selenium K-edge XANES spectra of amorphous red and gray selenium and from *B. subtilis* and the Kesterson bacillus after growth in a selenite medium. The spectra have been normalized to equivalent peak heights. The energy scales have been aligned with respect to the gray selenium absorption edge at 12658 eV.

crystalline modifications, all of which feature Se_8 rings and differ only in packing. The average ring Se-Se separation is 2.34 Å. The more common, amorphous form of red selenium consists of a mixture of distorted chains and Se_8 rings.

In view of the observed slight difference in the XANES spectra of gray and amorphous red selenium, EXAFS was employed in an attempt to distinguish the two forms. EXAFS was measured out to k of 12.7 $Å^{-1}$. The Fourier transform revealed a single frequency in both cases, which fit well with essentially the same parameters. Thus, the EXAFS results do not distinguish between the gray and red allotropes of elemental selenium.

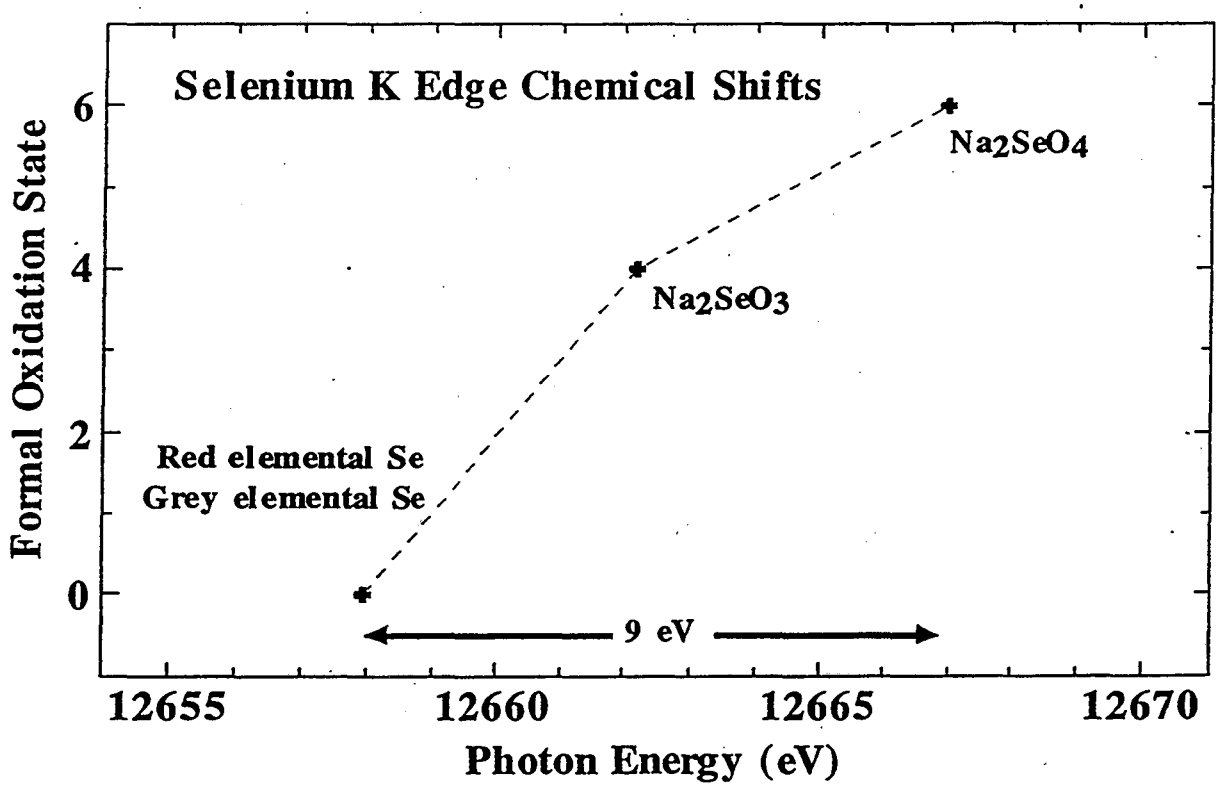

Figure 3. Chemical shifts at the Se K-edge.

Speciation of Tc in Wasteform Cement

^{99}Tc is a by-product of nuclear fission, and its long half-life ($t_{1/2}$ = $2.13x10^5$ years) necessitates its careful consideration in the long-term disposal of nuclear waste. The principal Tc-containing component of nuclear wastes is TcO_4^-. The propensity of TcO_4^- to migrate into the geosphere has led to research aimed at the facile conversion of pertechnetate into other, presumably less mobile compounds of ^{99}Tc (i.e., chemical reduction of the mobile TcO_4^- to less soluble Tc^{4+} species). One method for disposal involves microencapsulation of the liquid waste in a cement matrix with a reducing agents such as blast furnace slag (BFS). A preliminary XANES investigation of a process designed to reduce TcO_4^- to TcO_2 in wasteform cement has been described in Ref. 55. The line shapes of the XANES spectra and the chemical shifts of the Tc K-edge in TcO_4^-, TcO_2, and Tc metal were used to establish the oxidation state of Tc.

The Tc cements were prepared and packaged at LBNL. The Tc reference materials were prepared at both LBNL and LANL. The untreated cement was prepared by combining 50 wt.% Ordinary Portland Cement (OPC) and 50 wt.% of a simulated aqueous waste solution containing 1200 ppm $^{99}TcO_4^-$. The composition of the simulated wastestream has been reported

elsewhere.[56] The cement containing the reducing agent was composed of 10 wt.% simulated waste solution, 80 wt.% OPC, and 10 wt.% BFS. Slag is a source of reduced iron (ferrous ion) and complex reduced sulfides, which is believed to reduce TcO_4^- to TcO_2. The cement samples were cured for four days at 60°C. The TcO_2 reference material was prepared by the thermal decomposition of ammonium pertechnetate. The samples were contained in polyethylene tubes or polystyrene cuvettes, followed by the application of several heat sealed polyethylene film barriers.

XANES spectra were collected from cements prepared at LBNL, with and without slag, using a simulated nuclear waste stream spiked with pertechnetate ion. The XANES results of the Tc-containing cements and the Tc reference materials (Tc metal, TcO_2(IV), and a TcO_4(VII) solution) are presented in Figure 4. The range of chemical shifts for the Tc K-edge has been characterized and spans ~15 eV between the metallic and the Tc^{7+} state. The chemical shift from TcO_4^-(VII) to tetravalent TcO_2(IV) is -7 eV, therefore resolving the difference in oxidation state solely on the basis of edge position is relatively straightforward. Additionally, there is a characteristic pre-edge feature present in the TcO_4^- spectra that clearly fingerprints the tetrahedral TcO_4^- moiety. The spectra of Tc metal and TcO_2 have no such pre-edge features and exhibit edge positions significantly shifted to lower binding energies from that of TcO_4^-. Comparison of the XANES spectra of Tc in untreated cement (not shown-identical to that of the TcO_4^- spectra) to spectra of Tc

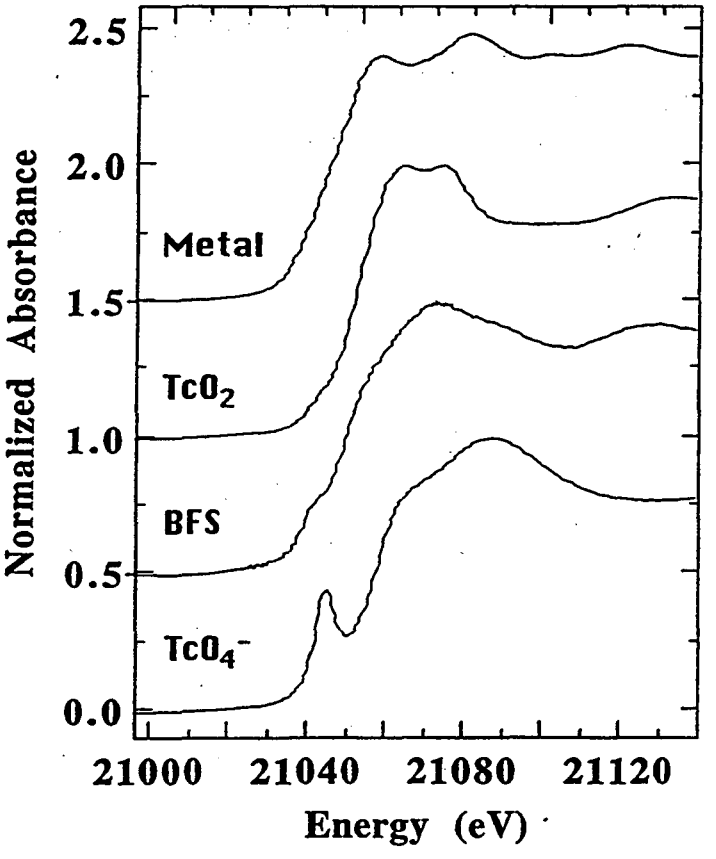

Figure 3. Normalized Tc K-edge XANES spectra of Tc model compounds (Tc metal, Tc dioxide, and Tc pertechnetate) and a spectrum from a single TcO_4^-/cement mixture cured at 60°C for four days with blast furnace slag (BFS). There was no reduction in mixtures consisting solely of Ordinary Portland Cement and TcO_4^- (spectra identical to TcO_4^-).

in slag treated cement, shows that the primary oxidation state of Tc in the cements is different. Several locations within the treated cement were characterized and the results were the same throughout. Thus, the addition of slag to the cement formulation, under these curing conditions, was essential to significantly reduce the TcO_4^- to TcO_2 (or some other Tc^{4+} compound) in thecement samples used in this investigation. The analysis of the EXAFS from the Tc metal and TcO_2 also provided some of the first detailed structural information about these materials. The full details of the results of the on-going Tc cement investigations will be covered in a future publication.

To complement the Tc cement studies, a XANES investigation on a wider range of model Tc compounds with formal oxidation states 0, +2, +4, +5 and +7 and an EXAFS characterization of the compounds $Tc_2(CO)_{10}$ and TcO_2 were performed.[57] Tc K-edge positions relative to NH_4TcO_4 are shown in Figure 5. There is a strong correlation between formal oxidation state and K absorption edge position. An increase in formal oxidation state implies an increase in effective charge, and it has been shown that x-ray absorption edge energies are governed mainly by the effective charge on the absorbing atom or ion. In general, chemical shifts are toward the high energy side of the elemental edge and increase progressively with the formal oxidation state of the absorbing atom. The ~15 eV K-edge shift between Tc metal and NH_4TcO_4 provides a substantial range over which the relationship of oxidation state to absorption edge energy may be examined. Of the eight systems studied, six display an almost linear relationship, with $Tc_2(CO)_{10}$ and $Tc(ArN)_3I$ showing more significant differences. $[TcCl_2(PR_2R')_2]_2$ and $TcCl_2py_4$ contain Tc as Tc(II), and their edge positions are 13.2 and 11.2 eV respectively lower than NH_4TcO_4. That $[TcCl_2(PR_2R')_2]_2$ has a 2.0 eV greater shift than $TcCl_2py_4$ may be a result of the stronger s-donor and weaker p-acceptor nature of PMe_2Ph versus C_5H_5N.

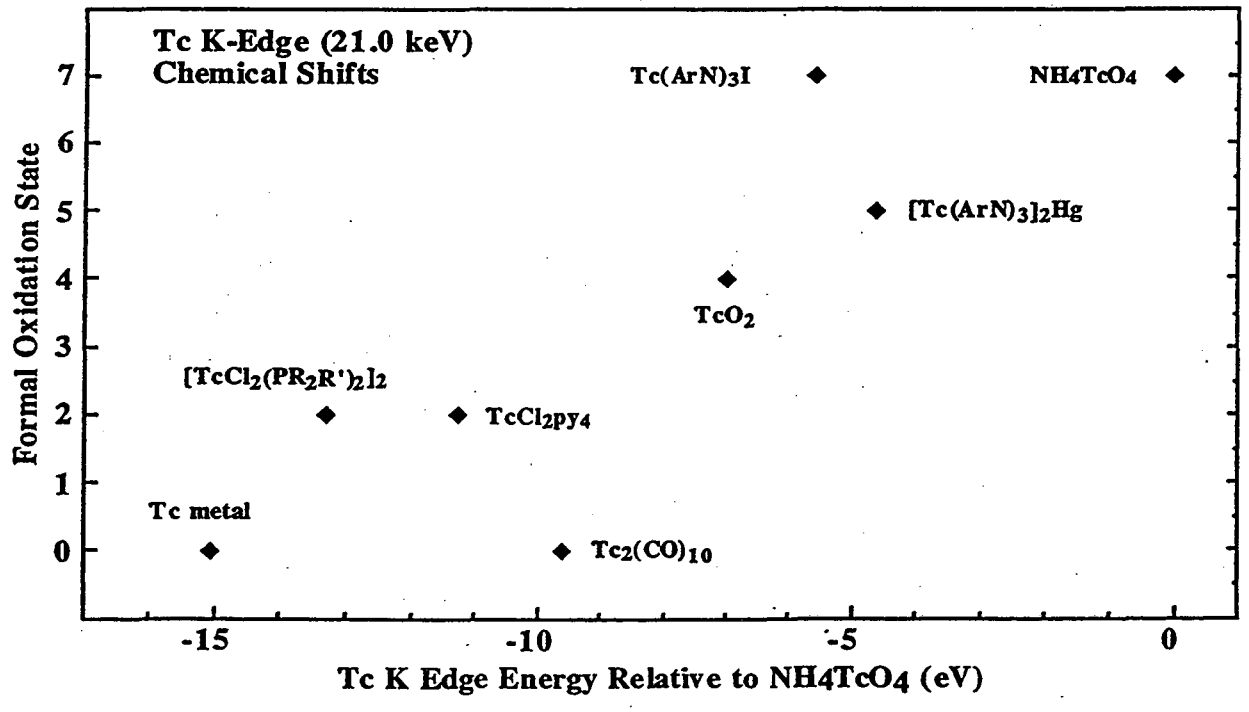

Figure 5. Chemical shifts at the Tc K-edge versus formal oxidation state for Tc metal, $[TcCl_2(PMe_2Ph)_2]_2$, $TcCl_2(py)_4$ (py=C_5H_5N), $Tc_2(CO)_{10}$, TcO_2, $Tc(ArN)_3I$ (ArN=2,6-$Pr^i_2C_6H_3N$), $[Tc(ArN)_3]_2Hg$, and NH_4TcO_4. All near edge spectra were collected with NH_4TcO_4 as a reference, and the chemical shifts are therefore reported relative to NH_4TcO_4.

Both $Tc(ArN)_3I$ and NH_4TcO_4 contain Tc in a formal oxidation state of +7, but $Tc(ArN)_3I$ has a Tc K-edge energy which is 5.6 eV lower than NH_4TcO_4. This is probably a reflection of the relative electron withdrawing properties of the ligands in each case, with the oxygens inducing a greater effective charge on the Tc than the ArN/I combination. The magnitude of the difference is somewhat surprising, as $Tc(ArN)_3I$ has an edge position which is further from NH_4TcO_4 than the Tc(V) $[Tc(ArN)_3]_2Hg$. In light of the preceding discussion, however, it is impossible to determine if this discrepancy is a genuine indication of differences in the effective charge at the metal atom. The most significant deviation from the formal oxidation state/K edge energy relationship is that of $Tc_2(CO)_{10}$, which has an edge position closer to NH_4TcO_4 than either $TcCl_2py_4$ or $[TcCl_2(PR_2R')_2]_2$. This is almost certainly the result of the electron withdrawing ability of the carbonyl unit, and indicates that *p* backbonding from metal to ligand dominates ligand to metal *s* donation.

Uranyl Ion Complexed With Tartaric, Citric, and Malic Acids

Actinide speciation information is essential for assessing and developing long-term strategies addressing problems such as migration in nuclear waste repositories or improvements in the processing of nuclear waste and materials. Relative to the latter, one method for removing uranium contamination from soils involves extraction using a chelating agent such as Tiron or citrate. Martell et al.[58,59] and Markovitz et al.[60] have published a series of articles detailing the complexation of the uranyl ion with tartaric, malic, and citric acids as a function of pH. From the analysis of potentiometric titration results, they showed that in the pH range 2-4, the uranyl ion forms a 2:2 dimeric species, $(UO_2)_2(L)_2$, where L= tartrate, malate, or citrate ligands. In considering the possible 2:2 structures shown in Fig. 6, both of which involve the α-hydroxyl group of the ligand(s) for bridging of the uranyl ions, Martell et al. stated a preference for the structure in the right panel Fig. 6.[59] However, it is not possible from the titration data to directly distinguish between the structures shown in Fig. 6 as well as other plausible 2:2 structures.

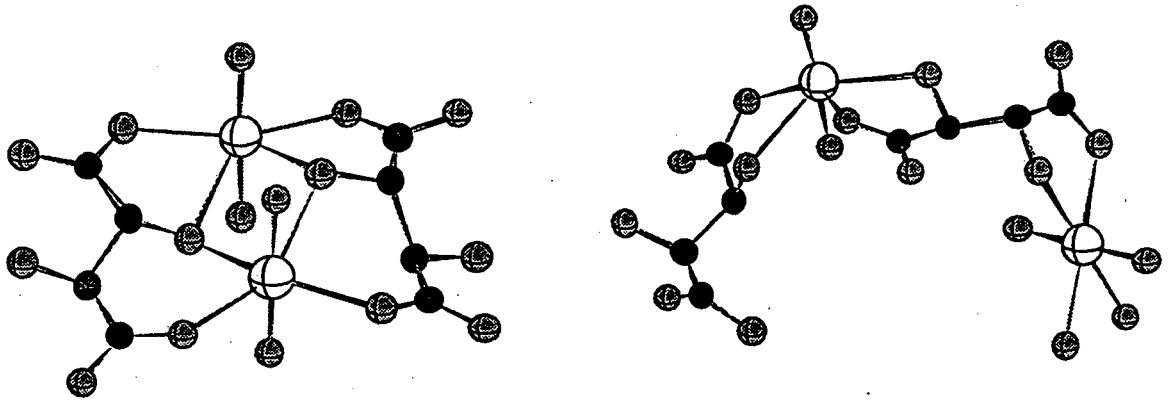

Figure 6. Possible structural models for the uranyl tartrate dimer having the empirical formula $(UO_2)_2(L)_2$ where L=tartrate; (left) uranyl groups are bridged by α-hydroxyl groups, (right) bridging occurs through a single α-hydroxyl group.

A 0.08 M stock solution of the UO_2^{2+} ion was used to prepare 1:1 mixtures of ligand to UO_2^{2+} ion. The final pH readings of the 0.04 M uranyl tartrate, malate, and citrate solutions were 2.2, 2.0, and 3.8, respectively. The raw k^3-weighted EXAFS data for the uranyl tartrate, malate, and citrate solutions show strong similarities in phase as well as amplitude. The FTs as shown in Fig. 7 (uncorrected for phase shift) illustrate that the EXAFS is dominated by scattering from the O atoms of the linear UO_2^{2+} group (peak at 1.30 Å) and scattering from the O atoms lying in the equatorial plane of the UO_2^{2+} ion (peak at 1.90 Å). In addition, the FTs show the presence of another interaction at *ca* 3.75 Å which is reproduced in each solution. The portion of the FT above

4 Å can be used to gauge the noise level in the EXAFS signal. Considering the fact that the FT above 4 Å is featureless and smooth, the 3.75 Å peak is the result of a real interaction, rather than an experimental artifact.

Modeling and curve-fitting analyses were performed on the raw EXAFS data to determine the bond lengths and coordination numbers, and to examine the origin of the peak at 3.75 Å. The data range used in the fitting procedure was 3-14 $Å^{-1}$ for the tartrate and malate solutions, and 3-12 $Å^{-1}$ for the citrate solution. Each sample shows ~N=2 oxygen atoms at 1.78 Å indicative of axial oxygen atoms on the uranyl group. A relatively weak multiple scattering (MS) interaction at 3.56 Å, originating from the 4-legged path along the O–U–O vector (twice the U–O_{ax} distance), was also included in the fits. Rather than being varied independently, this path was linked directly to floating bond lengths (R) and coordination number (*N*) values of the axial oxygen shell. The equatorial plane around the uranyl group contains ~N=2 oxygen atoms at *ca* 2.40 Å in each of the samples.

In an investigation of the nature of the 3.75 Å peak, this contribution was isolated by taking the difference between the uranyl tartrate data and a fit which included only the near-neighbor contributions mentioned above. The residual obtained by this procedure contains only those contributions unaccounted for in the fit-specifically the interaction appearing at 3.75 Å. The residual EXAFS signal was Fourier-filtered over the range of 3.2–4.2 Å to remove noise in the fit. Even at this level of analysis, the increasing EXAFS amplitude as a function of k is a signature of backscattering from an atom of relatively high Z. The corresponding single U shell fit confirms this assignment. The only other possible source of this peak would be scattering along paths involving the low Z ligands C or O centers. Low Z atoms are not normally detected in room temperature solutions at R>3 Å, unless a MS enhancement of the amplitude is operative. Examples for uranium systems have been observed when ligands like carbonate or nitrate adopt a symmetric bidentate geometry where the distal O atom is collinear with the absorbing atom and the C or N atoms. Thus, the most plausible alternative explanation for the peak at 3.75 Å is bidentate ligation of the carboxylate groups (i.e., a U–C_1–C_2 path). However, the phase and amplitude derived

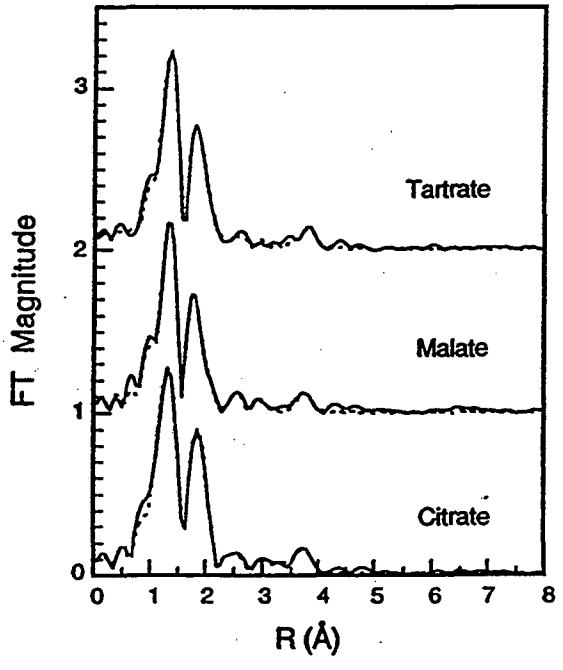

Figure 7. Fourier transforms (uncorrected for phase shift) of U L_{III} EXAFS for 1:1 mixtures of uranyl polycarboxylates. The solid line is the experimental data, and the dashed line corresponds to the best theoretical fit of the data. The U–U peak at 3.75 Å is evidence for the dimeric structure in the left panel of Fig. 6.

from a sum of 3-legged ($U \rightarrow C_1 \rightarrow C_2 \rightarrow U$) and 4-legged ($U \rightarrow C_1 \rightarrow C_2 \rightarrow C_1 \rightarrow U$) MS paths offer a poor match to the data. In addition, the resulting U–C_2 bond length of 4.24 Å would give the C_1–C_2 bond length at 1.31 Å which is inconsistent with the C–C bond length of 1.53 Å determined for $UO_2(CH_3COO)_2 \cdot 2H_2O$.

Apart from the structure shown in left panel of Fig. 6, the only other structure that could possess a U–U interaction at 3.95 Å would be a hydrolysis product, $(UO_2)_2(OH)_2^{2+}$. However, equilibrium calculations using the computer code HYDRAQL[61] and considering the numerous equilibria involved show that the concentrations of $(UO_2)_2(OH)_2^{2+}$ and other hydrolysis products are several orders of magnitude smaller than the concentration of $(UO_2)_2(L)_2$. Thus, combining the results with those of Martell et al.,[58,59] it is now possible to assign the structure in the left panel of Fig. 6 to the 2:2 dimer present in these solutions. The structure in the right panel of Fig. 6 is ruled out on the basis that a U–U interaction at 3.9 Å, if configurationally allowed, would not be detected due to dynamic disorder in the solution.

SYNCHROTRON RADIATION ENVIRONMENTAL WORK IN THE FUTURE

The utility of SR techniques in a wide range of environmental science applications, some of which have been briefly alluded to herein, clearly supports the contention that there will be a substantial amount of growth and influx of new users in this increasingly important field of SR. It is an understatement to mention that there are a significant number of existing environmental problems of national importance and the economic costs of remediating these problems is enormous. The scientific issues involved are challenging and the severity of many situations actually provides direct impetus for research motivated by potential future cost savings. It is clear to federal science funding agencies that there are significant benefits from performing both fundamental and applied research to support national environmental priorities. Similar to many other scientific fields at this time, the competition for research support is also very competitive. However, the future funding outlook is rather positive, a situation which differs markedly from that of many other disciplines. The utility of SR in environmental research, combined with the expanding research funding, has already led to increased research activities and promises to keep this type of work at the forefront of SR-based science in the near future.

A unique aspect of environmental SR work is that it is interdisciplinary and brings together scientists with widely different backgrounds to focus on a similar set of scientific issues at the end of a beamline. Many of the SR techniques and technologies have matured sufficiently to permit new environmental users to achieve a large degree of success without experiencing a lengthy start-up period. The impact that x-ray SR techniques can have on environmental research programs has been recognized by environmental research groups. These groups have rapidly utilized existing SR facilities to become one of the newest blocks of SR users. Rather than employing SR techniques as the sole means of experimental investigation, SR methods have been used to largely complement laboratory-based scientific methods.

There will be further growth areas within the envelope of SR environmental science. Other SR techniques such as x-ray scattering and standing waves,[62] will undoubtedly become important methodologies for examining specific environmental topics. The most important development may be the common use of experimental microscopy techniques to gain simultaneous spatial and x-ray absorption information. Emerging bioremediation programs will also utilize SR techniques to characterize the fundamental biological/chemical principles of bioremediation and to further develop bioremediation technologies.

The availability of beamtime at many of the best beamlines is quite limited, however the construction of third generation light sources along with the installation/improvement of beamlines at existing synchrotrons promises to make SR techniques more accessible for environmental studies. The inherent flux and brightness characteristics of the third generation sources will permit whole new classes of environmental experiments, until now not possible. Furthermore, the third generation sources are driving improvements in many areas (e.g. fluorescence detector developments) that will also enhance beamtime use at other facilities as well.

The x-ray synchrotron radiation light sources, cognizant of the needs and scientific requirements of the growing but diverse environmental science user community, have proposed the construction of new experimental beamline facilities dedicated to environmental science investigations. This is clearly demonstrated at the APS (Advanced Photon Source, located at Argonne National Laboratory) where there are a number of collaborative access team (CAT) beamlines organized and instrumented to investigate specific classes of scientific issues, a large number which are germane to the environmental sciences. There are also proposals to build new environmental beamline facilities at the ESRF (European Synchrotron Radiation Facility, located in Grenoble, France) and SSRL (Stanford Synchrotron Radiation Laboratory, located at the Stanford Linear Accelerator Center) storage rings to provide increased beamtime and capabilities for environmental studies. Both of these proposed facilities are to be built with the capabilities to safely handle radioactive and other hazardous materials.

Throughout the presentation and discussion herein, the focus has been on research conducted in the x-ray regime alone. Concomitant with the continued growth of environmental programs in the x-ray regime, there will be a corresponding breakthrough of environmental programs into the soft x-ray/vacuum ultraviolet (VUV) part of the spectrum. The development of environmental science programs utilizing VUV SR techniques has been limited to some degree by the ultra-high vacuum restriction of a complex electron spectrometer endstation. Many fundamental environmental processes take place at interfaces and VUV techniques have traditionally been used for the investigation of surface science phenomena. The development of fluorescence detection techniques, photoemission microscopes, and the possibilities of working behind windows (where vacuum restrictions are relaxed or unnecessary) will provide the means for working with "real" samples in the near future. As in the x-ray regime, many of these improvements will be made available by developments at third generation VUV sources such as the Advanced Light Source (ALS, located at Lawrence Berkeley National Laboratory).

CONCLUSIONS

The application of SR x-ray absorption spectroscopy techniques to a wide variety of scientific problems in the environmental sciences has proven to be extremely valuable for determining both oxidation state and local structural arrangements that are either difficult or impossible to obtain by other means. XAS is especially well-suited to environmental science investigations since materials may be examined *in-situ* and hazardous materials can be safely contained during experiments. This is clearly evident from the brief research synopses presented herein. As a result, the environmental science user belongs to one of the fastest growing segments of the SR community. The management of the SR sources has fully recognized the utility of SR techniques to environmental science programs and has made beamtime available to new users in this field. There have also been new, specialized beamline facilities proposed for several x-ray SR sources to provide additional beamtime dedicated to environmental science users. There will likely be a corresponding utilization of VUV techniques and VUV SR sources for environmental research in the near future. The advent of the third generation x-ray light source at the APS and the realization of environmental beamline facilities will provide new state-of the-art capabilities for environmental research. Thus, the future of SR environmental science is bright and will experience continued growth.

ACKNOWLEDGMENTS

This work was supported in part by the Director, Office of Energy Research, Office of Basic Energy Sciences, Chemical Sciences Division of the U.S. Department of Energy under Contract No. DE-AC03-76SF00098. The work was performed in part at SSRL and NSLS which are operated by the U.S. Department of Energy, Office of Basic Energy Sciences, Divisions of Chemical Sciences and Materials Science. The SSRL Biotechnology Program is supported by the

N.I.H., Biomedical Resource Technology Program, Division of Research Resources. Part of this work was also supported by the Bioremediation Education Science & Technology (BEST) Consortium at LBNL. NK would like to thank the EPSRC/NATO for a postdoctoral fellowship.

REFERENCES

1. R.G. Riley, J.M. Zachara, and F.J. Wobber, "Chemical Contaminants on DOE Lands and Selection of Contaminant Mixtures for Subsurface Science Research," **1992**, DOE/ER-0547T.
2. J.D. Spencer, editor, "Remediation, "Chapter V in: Joint DOE-EPA Report on Collaborative Environmental Research, **1993**.
3. H. Nitsche, *J. Alloys and Compounds*, to be published.
4. R. Prins and D.E. Koningsberger, "X-ray Absorption: Principles, Applications, Techniques for EXAFS, SEXAFS, and XANES", Wiley, New York, 1988.
5. P.A. Lee, P.H. Citrin, P. Eisenberger, and B. M. Kincaid, *Rev. Mod. Phys.* **1981**, *53*, 769.
6. J.R. Helliwell, *Reports on Prog. in Phys.* **1984**, *47*, 1403-1497.
7. J. Mustre de Leon, J.J. Rehr, S. Zabinsky, and R.C. Albers, *Phys. Rev.* B, **1991**, *44*, 4146.
8. Graham. N. George, EXAFSPAK computer code program suite, SSRL, (1994).
9. E. Stern and S. Heald, *Rev. Sci. Instr.* **1979**, *59*, 1579.
10. W.K. Warbuton, *Nucl. Instr. and Meth.* **1986**, *A246*, 541.
11. S.P. Cramer, O. Tench, M. Yocum, and G.N. George, *Nucl. Instr. and Meth.* **1988**, *A266*, 586.
12. J.J. Bucher, P.G. Allen, N.M. Edelstein, D.K. Shuh, N.W. Madden, C. Cork, P. Luke, D. Pehl, and D. Malone, to be submitted to Rev. Sci. Instrum.
13. K.F. Hayes, A.L. Roe, G.E. Brown Jr., K.O Hodgson, J.O. Leckie, and G.A. Parks, *Science,* **1987**, *238*, 783.
14. L.J. Pickering, G.E. Brown, Jr., and T. Tokunaga, "X-ray Absorption Spectroscopy of Selenium-contaminated Soils," Stanford Synchrotron Radiation Laboratory Activity Report, 1993, p. 92.
15. C.J. Chisholm-Brause, P.A. O'Day, G.E. Brown, Jr., and G.A. Parks, *Nature*, **1990**, *348*, 528.
16. C.J. Chisholm-Brause, G.E. Brown, Jr., and G. A. Parks, *XAFS VI Sixth International Conference on X-ray Absorption Fine Structure*, 1991, (ed. S.S. Hasnain), New York: Ellis Horwood Ltd, Publishers, pp. 263-265.
17. P.A. O'Day, G.E. Brown, Jr., and G.A. Parks, *XAFS XAFS VI Sixth International Conference on X-ray Absorption Fine Structure*, 1991, (ed. S.S. Hasnain), New York: Ellis Horwood Ltd, Publishers, pp. 260-262.
18. P.A. O'Day, G.A. Parks, and G.E. Brown, Jr., *Clays and Clay Minerals*, **1994**, *42*, 337.
19. P.A. O'Day, G.E. Brown, Jr., and G.A. Parks, *J. Colloid and Inter. Sci.*, **1994**, *165*, 269.
20. K.F. Hayes, L.E. Katz, and J.E. Penner-Hahn, "XAS Study of Metal/Ion Partitioning at Water/Mineral Interfaces," Stanford Synchrotron Radiation Laboratory Activity Report, 1993, p. 96.
21. G. Bidoglio, P.N. Gibson, M. O'Gorman, and K.J. Roberts, *Geochim. Cosmochim. Acta,* **1993**, *57*, 2389.
22. L. Charlet and A.J. Manceau, *Colloid and Inter. Sci.*, **1992**, *148*, 443.
23. S.E. Fendorf, G.M. Lamble, M.G. Stapleton, M.J. Kelley, and D.L. Sparks, *Environ. Sci. Technol.,* **1994**, *28*, 284.
24. C.J. Chisholm-Brause, K.F. Hayes, A.L. Roe, G.E. Brown, Jr., G.A. Parks, J.O. Lekie, *Geochim. Cosmochim. Acta,* **1990**, *54*, 1897.
25. A.L. Roe, K.F. Hayes, C.J. Chisholm-Brause, G.E. Brown, Jr., G.A. Parks, K.O. Hodgson, and J.O. Leckie, *Langmuir*, **1991**, *7*, 367.

26. J.E. Silk, L.D. Hansen, D.J. Eatough, M.W. Hill, N.F. Mangelson, F.W. Lytle, and R.B. Greegor, *Physica B*, **1989**, *158*, 247.
27. F.E. Huggins, J. Zhao, N. Shah, F. Lu, and G.P. Huffman, *Energy and Fuels*, **1993**, *7*, 482.
28. A. Vairavamurthy, W. Zhou, and B. Manowitz, "Speciation of Chromium, Nickel, and Copper in Anoxic Sediments: Effects of Hydrogen Sulfide and Thiols," National Synchrotron Light Source Annual Report, Brookhaven National Laboratory, 1992.
29. N.E. Pingitore, F.W. Lytle, B.M. Davies, M.P. Eastman, P.G. Eller, and E.M. Larson, *Geochim. Cosmochim. Acta*, **1992**, 56, 1531.
30. S.C. Kohn, J.M. Charnock, C.M.B. Henderson, and G.N. Greaves, *Contributions to Mineralogy and Petrology*, **1990**, *105*, p. 359.
31. P.G. Allen, J.M. Berg, C.J. Chisolm-Brause, S.D. Conradson, R.J. Donohoe, D.E. Morris, J.A. Musgrave, C.D. Tait, "Determining Uranium Speciation in Contaminated Soils by Molecular Spectroscopic Methods: Examples from the Uranium in Soils Integrated Demonstration." (Waste Management '94 Meeting Proceedings, Tucson, AZ.)
32. P.M. Bertsch, D.B. Hunter, S.R. Sutton, S. Bajt, M.L. Rivers, *Environ. Sci. Technol.* **1994**, *28*, 980.
33. C.J. Chisholm-Brause, S.D. Conradson, C.T. Buscher, P.G. Eller, and D.E. Morris, *Geochim. Cosmochim. Acta*, **1994**, *58*, 3625.
34. A.J. Dent, J.D.F. Ramsay, and S.W. Swanton, *J. Colloid and Interface Sci.*, **1992**, *150*, 45.
35. A.J. Francis, C.J. Dodge, F. Lu, G.P. Halada, and C.R. Clayton. *Environ. Sci. Technol.*, **1994**, *28*, 636.
36. F. Farges, C.W. Ponader, G. Calas, and G.E. Brown, Jr., *Geochim. Cosmochim. Acta.*, **1992**, *56*, 4205.
37. P.G. Eller, G.D. Jarvinen, J.D. Purson, R.A. Penneman, R.R. Ryan, F.W. Lytle, and R.B. Greegor, *Radiochim. Acta*, **1985**, *39*, 17.
38. E.M. Larson, F.W. Lytle, P.G. Eller, R.B. Greegor, and M.P. Eastman, *J. Noncryst. Solids*, **1990**, *116*, 57.
39. G.S. Knapp, B.W. Veal, D.J. Lam, A.P. Paulikas, and H.K. Pan, *Mater. Lett.*, **1984**, *2*, 253.
40. J. Petiau, G. Calas, T. Dumas, and A.M. Heron, in: *EXAFS and Near-Edge Structure III*,Springer Proceedings in Physics, Vol. 2, eds. K.O. Hodgson et al., **1984**, Springer-Verlag, New York, p. 291.
41. G.S. Knapp, B.W. Veal, A.P. Paulikas, A.W. Mitchell, D.J. Lam, and T.E. Klippert, in: *EXAFS and Near-Edge Structure III*, Springer Proceedings in Physics, Vol. 2, eds K.O. Hodgson et al., **1984**, Springer-Verlag, New York, p. 305.
42. N.T. Barret, G.M. Antonini, F.R. Thornley, G.N. Greaves, and A. Manara, *Mat. Res. Soc. Symp. Proc.* **1987**, Vol. 84, p. 571; F.R. Thornley, N.T. Barret, G.N. Greaves, and G.M. Antonini, *J. Phys. C: Solid State Phys.*, **1986**, *19*, L563.
43. J.-M. Combes, C.J. Chisholm-Brause, G.E. Brown, Jr., G.A. Parks, S.D. Conradson, P.G. Eller, I. Triay, D.E. Hobart, and A. Meier, *Environ. Sci. Technol.*, **1992**, *26*, 376.
44. J. Petiau, G. Calas, D. Petitmaire, A. Bianconi, M. Benfatto, and A. Marcelli, *Phys. Rev. B*, **1986**, *34*, 7350.
45. G. Kalkowski, G. Kaindl, S. Bertram, G. Schmiester, J. Rebizant, J.C. Spirlet, and O. Vogt, O. *Solid State Comm.*, **1987**, *64*, 193.
46. G. Kalkowski, G. Kaindl, W.D. Brewer, and W. Krone, *Phys. Rev. B*, **1987**, *35*, 2667.
47. S. Bertram, G. Kaindl, J. Jove, M. Pages, J. Gal, *Phys. Rev. Lett.*, **1989**, *63*, 2680.
48. D.K. Veirs, C.A. Smith, J.M. Berg, B.D. Zwick, S.F. Marsh, P.G. Allen, and S.D. Conradson, *J. Alloys and Compounds*, **1994**, *213*, 328.
49. L.E. Cox, R. Martinez, J.H. Nickel, S.D. Conradson, and P.G. Allen, *Phys. Rev. B*, **1995**, *51*, 751.
50. F.A. Tomei, L.L. Barton, C.L. Lemanski, and T.G. Zocco, *Can. J. Microbiol.*, **1992**, *32*, 1328.

51. R.S. Oremland, J.T. Hollobaugh, A.S. Maest, T.S. Presser, L.G. Miller, and C.W. Culbertson, *Appl. Environ. Microbiol.*, **1994**, *55*, 2333.
52. B.B. Buchanan, T. Leighton, J. Liu, B.C. Yee, S. Jovanovich, A. Yee, W.-S. Yang, S. Ekune, and B. Chapman, in *Abstracts of Fifth International Symposium on Selenium in Biology and Medicine;* Vanderbilt University School of Medicine, Nashville, TN, **1992**, p 30.
53. A.O. Summers and S. Silver, *Ann. Rev. Microbiol.*, **1978**, *32*, 637.
54. D.R. Lovley, *Ann. Rev. Microbiol.*, **1993**, *47*, 263.
55. D. K. Shuh, N. Kaltsoyannis, J. J. Bucher, N. M. Edelstein, S. B. Clark, H. Nitsche, T. Reich, E. A. Hudson, I. Almahamid, P. Torretto, W. Lukens, K. Roberts, B. C. Yee, D. E. Carlson, A. Yee, B. B. Buchanan, T. Leighton, W.-S. Yang, and J. C. Bryan, *Mater. Res. Soc. Symp. Proc.*, **1994**, *344*, 323.
56. S. Bajt, S.R. Sutton, M.L. Rivers, and J.V. Smith, *Anal. Chem.*, **1993**, *65*, 1800.
57. I. Almahamid, J. J. Bucher, J. C. Bryan, S. B. Clark, N. M. Edelstein, E. A. Hudson, N. Kaltsoyannis, H. Nitsche, T. Reich, P. Torretto, W. Lukens, K. Roberts, and D. K. Shuh, *Inorg. Chem.*, **1995**, *34*, 193.
58. K.S. Rajan, and A.E. Martell, *J. Inorg. Nucl. Chem.*, **1964**, *26*, 1927.
59. K.S. Rajan and A.E. Martell, *Inorg. Chem.*, **1965**, *4*, 462.
60. G. Markovits, P. Klotz, and L. Newman, *Inorg. Chem.*, **1972**, *11*, 2405.
61. C. Papelis, K.F. Hayes, and J.O. Leckie, *HYDRAQL: A Program for the Computation of Aqueous Batch Systems Including Surface Complexation Modeling of Ion Adsorption at the Oxide/Solution Interface*: Tech. Rep. 306, Dept. of Civil Eng., Stanford Univ, 1988.
62. Y. Qian, N.C. Sturchio, R.P. Chiarello, P.F. Lyman, T.L. Lee, and M.J. Bedzyk, *Science*, **1994**, *265*, 1555.

LAWRENCE BERKELEY NATIONAL LABORATORY
UNIVERSITY OF CALIFORNIA
TECHNICAL & ELECTRONIC INFORMATION DEPARTMENT
BERKELEY, CALIFORNIA 94720